CSEM, TOPAS and Echo Sounder survey of the Southern Hikurangi Margin 1st – 13th November 2020: *RV Tangaroa* TAN2012 voyage report

P Kannberg
J Perez
L Boettger
KF Kroeger
S Woelz
F Turco
IA Pecher
C Ray
T Hill
C Armerding
R King

GNS Science Report 2021/11
May 2021

GNS SCIENCE
TE PŪ AO

DISCLAIMER

BIBLIOGRAPHIC REFERENCE

Kannberg P, Kroeger KF, Pecher IA, Armerding C, Perez J, Woelz S, Ray C, King R, Boettger L, Turco F, Hill T. 2021. CSEM, TOPAS and Echo Sounder survey of the Southern Hikurangi Margin 1st – 13th November: *RV Tangaroa* TAN2012 voyage report. Lower Hutt (NZ): GNS Science. 32 p. (GNS Science report; 2021/11). doi:10.21420/VJZ0-2Y67.

P Kannberg, Scripps Institution of Oceanography, 9500 Gilman Drive, La Jolla CA 92093, USA

KF Kroeger, GNS Science, PO Box 30368, Lower Hutt 5040, New Zealand

IA Pecher, University of Auckland, Private Bag 92019, Auckland 1142, New Zealand

C Armerding, Scripps Institution of Oceanography, 9500 Gilman Drive, La Jolla CA 92093, USA

J Perez, Scripps Institution of Oceanography, 9500 Gilman Drive, La Jolla CA 92093, USA

S Woelz, National Institute of Water & Atmospheric Research, Private Bag 14901, Wellington, 6241, New Zealand

C Ray, National Institute of Water & Atmospheric Research, Private Bag 14901, Wellington, 6241, New Zealand

R King, Scripps Institution of Oceanography, 9500 Gilman Drive, La Jolla CA 92093, USA

L Boettger, University of Auckland, Private Bag 92019, Auckland 1142, New Zealand

F Turco, University of Otago, PO Box 56, Dunedin 9054, New Zealand

T Hill, University of Otago, PO Box 56, Dunedin 9054, New Zealand

www.gns.cri.nz

ISSN 2350-3424 (online)
ISBN 978-1-99-001077-4 (online)
http://dx.doi.org/10.21420/VJZ0-2Y67

CONTENTS

FIGURES

TABLES

ABSTRACT

The TAN2012 voyage took place between the 1st and 13th of November 2020 aboard *RV Tangaroa*. Controlled source electromagnetic (CSEM) data, multibeam bathymetry, single-beam echo sounder, water column and TOPAS sub-bottom profile data were collected at the southern end of the Hikurangi subduction margin. CSEM profiles were collected along existing regional 2D reflection seismic lines to characterise and quantify gas and gas hydrate accumulations in the sub-seafloor. Multibeam bathymetry and water column data, as well as single-beam echo sounder data, were acquired in tandem with CSEM data. The hydro-acoustic datasets supplement and expand on data from earlier voyages. A high-resolution TOPAS dataset was collected to further characterise an active seep site. This report describes the background and technical procedures of data collection during the voyage.

KEYWORDS

Gas hydrate; Hikurangi Margin; Controlled source electromagnetics (CSEM); HYDEE; Methane; Digital Scientific Media Library ID U00095

This page left intentionally blank.

1.0 THE HYDEE RESEARCH PROGRAMME AND TAN2012

In 2017, the New Zealand Ministry for Business, Innovation & Employment approved funding of a five-year research programme entitled 'Economic Opportunities and Environmental Implications of Energy Extraction from Gas Hydrates'. The acronym for this programme is HYDEE. The HYDEE programme poses two high-level questions that are essential to address if New Zealand is to consider the extraction of gas from gas hydrates for the purposes of energy supply. These questions are:

1. Will feasible hydrocarbon production scenarios, either directly from gas hydrates or through gas hydrates, significantly impact seafloor stability, ecology or ocean biogeochemistry (Figure 1.1)?
2. What are the likely socioeconomic implications of gas hydrate production in New Zealand?

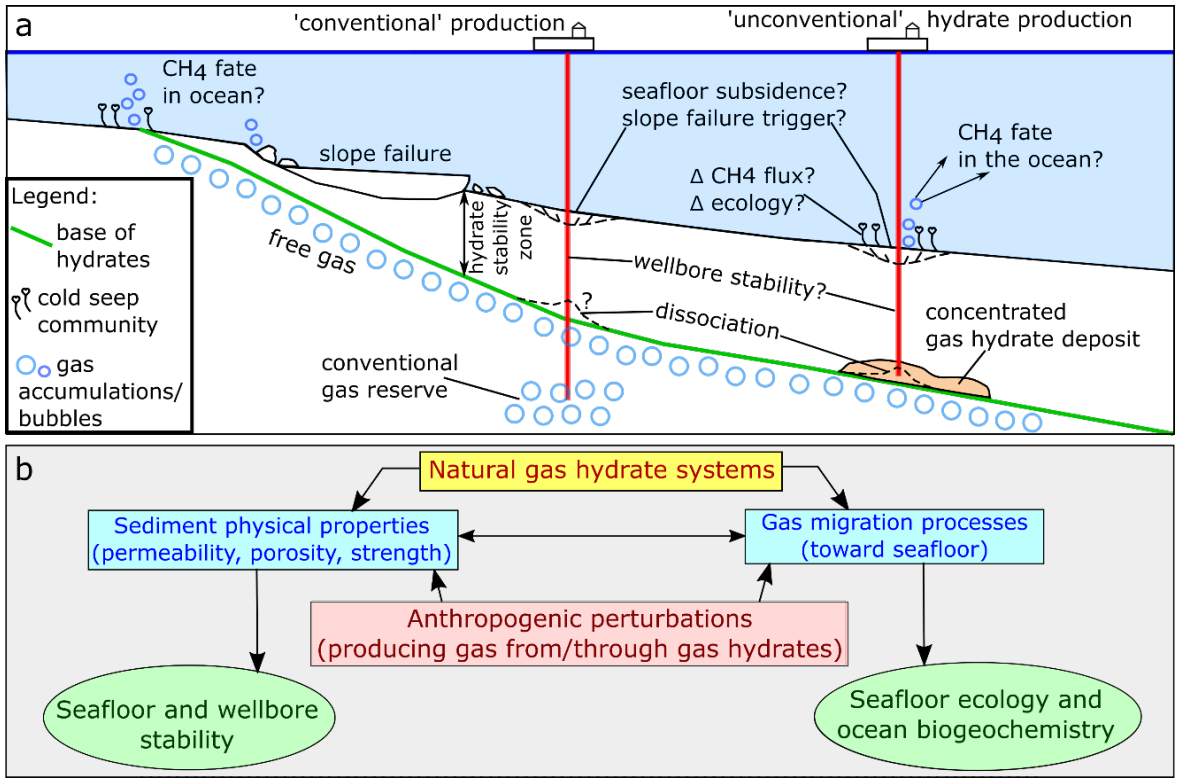

Figure 1.1 (A) Schematic of geological, ecological and biogeochemical processes in marine gas hydrate environments. Two hypothetical production scenarios are shown: one for conventional gas beneath hydrates, one for 'unconventional' gas hydrates. (B) The influence of natural gas hydrates on sediment physical properties and gas migration processes, which thereby effect seafloor stability, ecology and biogeochemistry. Anthropogenic gas hydrate perturbations overprint the influences of the natural system.

These two high-level questions are being addressed via four core Research Aims:

- (RA1.1) Determine New-Zealand-specific frameworks (geological and economic) for energy production from (and through) gas hydrates.
- (RA1.2) Predict the geo-mechanical responses at the seafloor and wellbore induced by production drilling.
- (RA1.3) Investigate the impact that changes in seafloor stability and/or methane flux could have on marine ecosystems.
- (RA1.4) Incorporate Vision Mātauranga and deliberative community engagement into gas hydrate science to explore potential for growth of Māori economies and broad socioeconomic implications of resource extraction.

TAN2012 is the third research voyage to be co-funded under the HYDEE research programme. The voyage is also funded by the United States National Science Foundation (NSF) through a funding grant to Steven Constable and Peter Kannberg of the University of California, San Diego. Data collected during TAN2012 helps us to address RA 1.1 of the HYDEE programme. The voyage addressed nine specific objectives set out in the funded NSF project (see Section 4).

2.0 GEOLOGICAL SETTING

The research area for TAN2012 lies at the southern end of the Hikurangi subduction margin, in a region where the Pacific Plate subducts obliquely beneath the Australian Plate (Figure 2.1). Subduction leads to pronounced folding and faulting of sediments and to focused fluid flow and the formation of gas hydrates close to the seafloor. These gas hydrates, ice-like substances of gas enclosed in a rigid cage of water molecules, are stable at relatively low temperatures and high pressures – conditions that are met in water depths greater than ~650 m in this part of the world.

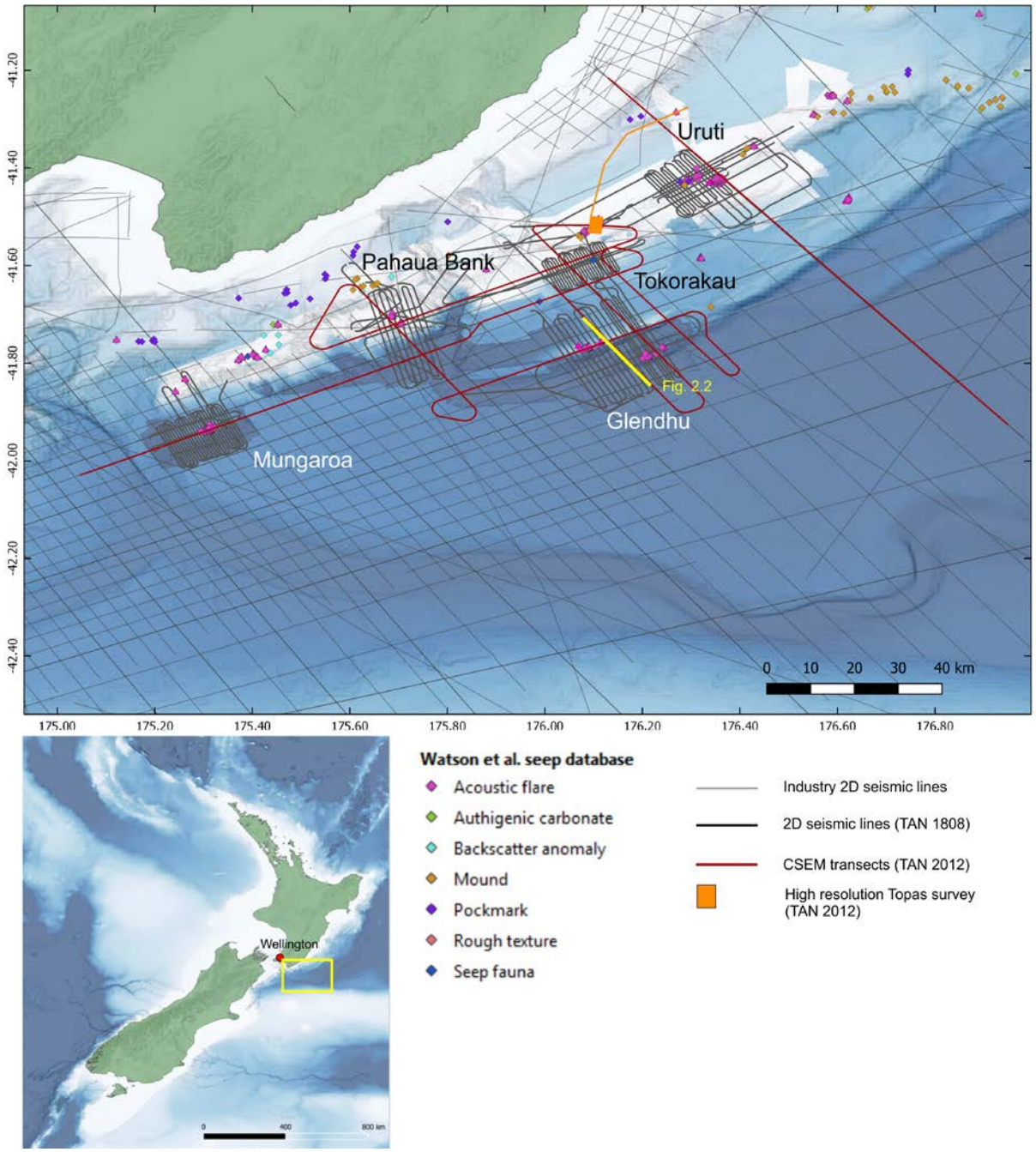

Figure 2.1 Overview of the surveyed area at the Hikurangi Margin during TAN2012, showing regional 2D seismic lines and survey areas of the TAN2018 voyage (Crutchley et al. 2018b).

Gas hydrates are most commonly identified over large areas from characteristic seismic reflections known as bottom simulating reflections (BSRs; Figure 2.2). BSRs are widely observed on the Hikurangi subduction margin and have been used to map out the regional distribution of gas hydrates (Pecher and Henrys 2003) and their relationship to tectonic deformation (Barnes et al. 2010). Beyond BSRs, concentrated accumulations of gas hydrates have been identified from anomalously high seismic reflectivity and seismic velocities (Crutchley et al. 2015; Fohrmann and Pecher 2012; Fraser et al. 2016). However, BSRs and other characteristics encountered in reflection seismic data are, at best, imperfect indicators of hydrate presence and concentration. In the Gulf of Mexico, Majumdar et al. (2016) found that, of 35 BSR-intersecting wells, only 13 were interpreted to have hydrate-bearing sediments, a rate of only 37%. Furthermore, prior controlled source electromagnetic (CSEM) surveys have found that, while some increase in resistivity (caused by the presence of hydrate) can be found collocated with BSRs, the strongest resistors did not correlate with BSR presence (e.g. Kannberg and Constable 2020).

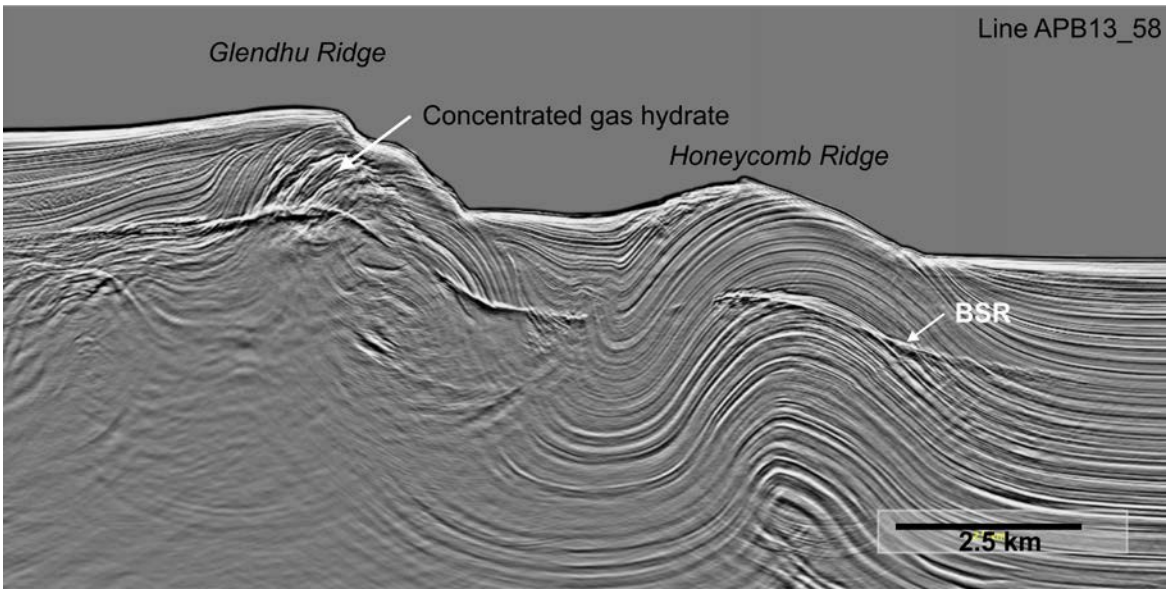

Figure 2.2 Part of seismic line APB13_58 across Glendhu and Honeycomb ridges selected for a parallel CSEM transect with pronounced BSR and gas-hydrate-related reflection anomalies.

Seafloor pockmarks are widespread on the margin (Watson et al. 2019), marking locations of vigorous gas escape at the seafloor. Such sites of focused gas escape can be linked to sub-surface gas hydrate accumulations (Plaza-Faverola et al. 2014). Venting is particularly common above faults, structural culminations and ridges related to convergent margin deformation (Barnes et al. 2010). Gas sampling suggests that both biogenic and thermogenic sources of gas are present along the southern Hikurangi Margin (Greinert et al. 2010; Fugro Marine Geoservices 2015). Thermogenic gas is likely generated from sedimentary strata subducting beneath the accretionary wedge (Kroeger et al. 2015). In the cool subduction margin thermal regime, abundant generation of microbial methane also occurs beneath the interval where gas hydrates are stable. Focusing of gas into anticlinal structures results in concentrated gas hydrate and free gas accumulations (Crutchley et al. 2018a; Kroeger et al. 2019). Therefore, the southern end of the margin is an ideal location to study relationships between tectonics, gas migration, gas hydrate formation and methane seepage.

3.0 SCIENTIFIC PARTICIPANTS

Peter Kannberg	Scripps Institution of Oceanography
Karsten Kroeger	GNS Science
Ingo Pecher	University of Auckland
Chris Armerding	Scripps Institution of Oceanography
Jake Perez	Scripps Institution of Oceanography
Roz King	Scripps Institution of Oceanography
Chris Ray	NIWA (National Institute of Water & Atmospheric Research)
Susi Woelz	NIWA (National Institute of Water & Atmospheric Research)
Francesco Turco	University of Otago
Laurenz Boettger	University of Auckland
Tayla Hill	University of Otago

Figure 3.1 Voyage participants from left to right: Peter Kannberg, Ingo Pecher, Chris Ray, Karsten Kroeger, Chris Armerding, Susi Woelz, Laurenz Boettger, Tayla Hill, Roz King and Francesco Turco. Added post-production: Jake Perez, who was operating the deep-tow winch at the time.

4.0 TAN2012 SCIENTIFIC OBJECTIVES

TAN2012 has focused on the collection of controlled-source electromagnetic data that help us to quantify gas and gas hydrate occurrence and to characterise the way in which gas hydrates are forming in the deforming wedge of the Hikurangi subduction margin. The voyage objectives were to:

1. Determine gas hydrate distribution and saturation from resistivity data along the length of a deforming accretionary wedge, using high-quality seismic data to constrain and jointly interpret the CSEM results.
2. Provide new constraints on the relative volumes of sediment hosting low (<10% of pore space) and high (>40% of pore space) gas hydrate saturations.
3. Test the working model (Crutchley et al. 2018a) that gas hydrates are significantly more concentrated in landward-dipping strata of the wedge than in seaward-dipping strata.
4. Determine the role that faulting plays in the distribution of gas hydrates. For example, do broad zones of proto-thrusts (common features of the Hikurangi wedge) influence the distribution and concentration of gas hydrates?
5. Provide better understanding on the discrepancies between seismic-derived and CSEM-derived estimations of gas hydrate saturation by considering evidence for free gas co-existing in the hydrate stability zone with concentrated gas hydrate deposits.
6. Constrain the concentration and distribution of free gas beneath the hydrate system in areas where seismic ‘flat spots’ suggest the existence of interconnected gas columns.
7. Investigate whether concentrated gas hydrates above such gas columns have formed via vigorous gas ‘injection’ from these gas reservoirs, or whether the gas reservoirs accumulated after the formation of gas hydrates (for example, if the hydrates formed from dissolved in-situ methane).
8. How much gas hydrate is in the region around the ‘feather edge’ of gas hydrate stability?
9. How sensitive is this gas hydrate to dissociation caused by ocean warming?

5.0 SUMMARY OF ACTIVITIES

Friday 30 October to Saturday 31 October

Mobilisation – port of Wellington.

Sunday 1 November

13:30 – Leaving port of Wellington.

Monday 2 November

3:00 – Start deployment of CSEM gear, start recording at 10:00 hours west of Mungaroa. Initially dynamic positioning running, shut down later; multibeam echo sounder (MBES), TOPAS and single-beam echo sounder (SBES) running. Power failure when crossing Mungaroa seep sites. Note 15-minute data gap over Mungaroa in CSEM data.

Tuesday 3 to Saturday 7 November

Running CSEM, MBES, TOPAS and SBES along planned lines (see Section 6).

Sunday 8 November

10:00 – Recovery of CSEM gear ahead of bad weather; run MBES, TOPAS and SBES across seep and sand wave site north of Tokorakau, initially as NW–SE survey lines.

Monday 9 November

Run MBES, TOPAS and SBES across seep and sand wave site north of Tokorakau, initially as NW–SE survey lines; beginning of high-resolution TOPAS across seep at 50 m offset across the centre of the area.

Tuesday 10 November

Continue with high-resolution TOPAS with MBES and SBES across seep sites.

Wednesday 11 November

Weather has calmed down; deploy CSEM gear and start recording at 5:00 north of Uruti Ridge.

Thursday 12 November

Finished survey line southwest of Uruti Ridge; recovery of CSEM gear.

Friday 13 November

Return to Port of Wellington; arrival 8:00.

6.0 SURVEY AREA AND LAYOUT

Transects for CSEM acquisition were focused on areas where results of the TAN1808 voyage (Crutchley et al. 2018b) and available 2D seismic data show indications for subsurface hydrate accumulations, presence of gas charged sediments and gas seepage. The survey was carried out along long-offset industrial seismic lines to allow for comparison between long-offset seismic-data-derived gas hydrate saturation estimates and the CSEM results (Figure 2.1).

In addition, a detailed sub-bottom profile (TOPAS), multibeam bathymetry and single-beam water column survey was carried out over an area north of the Tokorakau site (Figure 2.1) that was mapped in detail during the TAN1808 voyage (Figure 6.1).

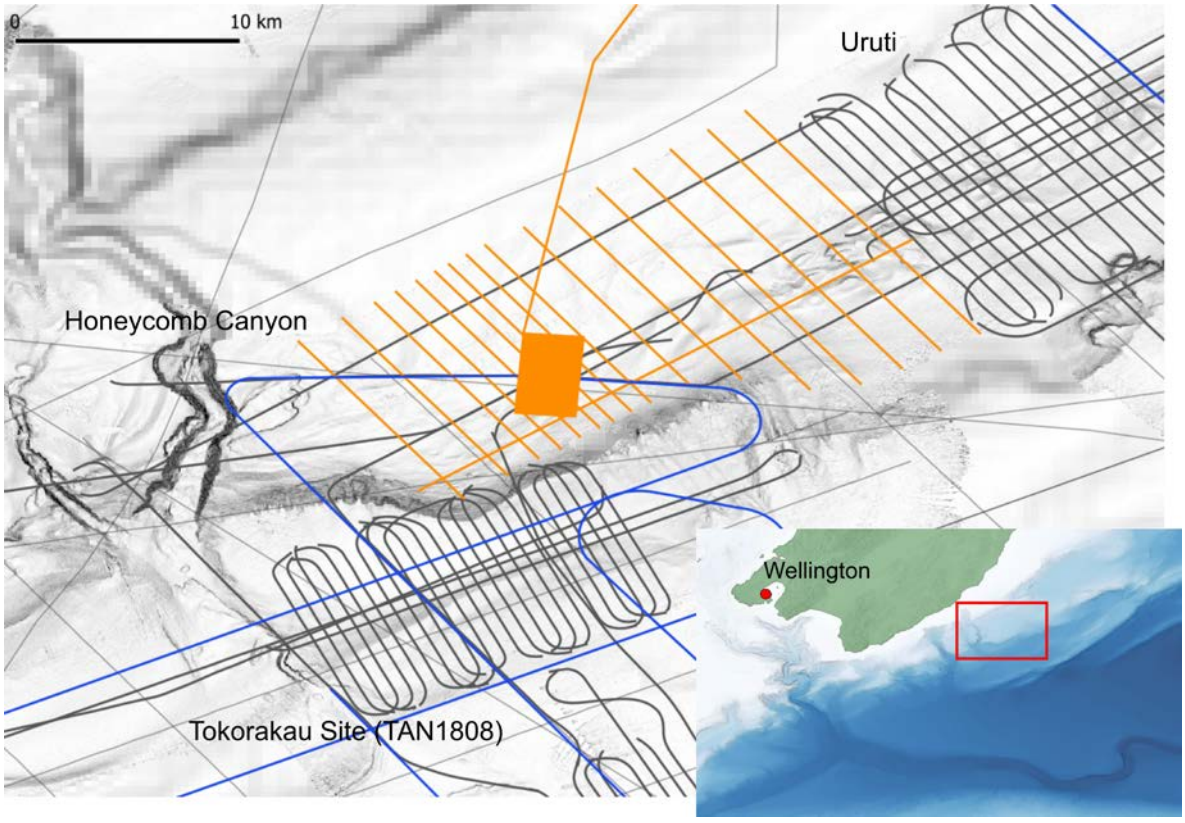

Figure 6.1 High-resolution TOPAS survey area and lines (orange), CSEM survey lines (blue), TAN1808 seismic surveys (black lines) and regional industry seismic data (grey) plotted on bathymetric relief.

7.0 SURVEY EQUIPMENT, METHODOLOGY AND DATA

7.1 Controlled Source Electromagnetics

While high-frequency magnetotelluric signals are usable in resistive terrestrial environments, in the marine environment, the conductive seawater attenuates high-frequency signals. The loss of those frequencies limits the ability of the magnetotelluric method to accurately resolve shallow resistivity structures. To mitigate this effect, a transmitter is used to re-transmit a portion of those missing frequencies into the marine environment just above the seafloor. There, the transmitted current is well coupled to the seafloor and little electric field strength is attenuated in seawater. However, while the conductive seawater attenuates signal, it also allows for large electric currents to be transmitted and attenuates magnetotelluric and man-made noise in the CSEM frequency spectrum.

The basic methodology of the CSEM method is to tow a transmitter just above the seafloor and then record its transmitted signal on stationary seafloor or towed receivers. CSEM methods are sensitive to pore fluid conductivity and are increasingly being used to identify and quantify electrically resistive gas hydrate deposits in seafloor sediments. SUESI (Scripps Undersea Electromagnetic Source Instrument) is a deep-towed transmitter used for CSEM. The CSEM method of ocean survey utilises a deep-towed electric field dipole that emits a signal that penetrates the seabed (Figure 7.1). The signal is measured by receivers (called Vulcans) towed through the water behind the dipole transmitter. The transmitted signal is modified by the electrical conductivity of the surrounding environment. Conductive environments attenuate the signal, while resistive environments (such as hydrate-bearing sediments) preserve it.

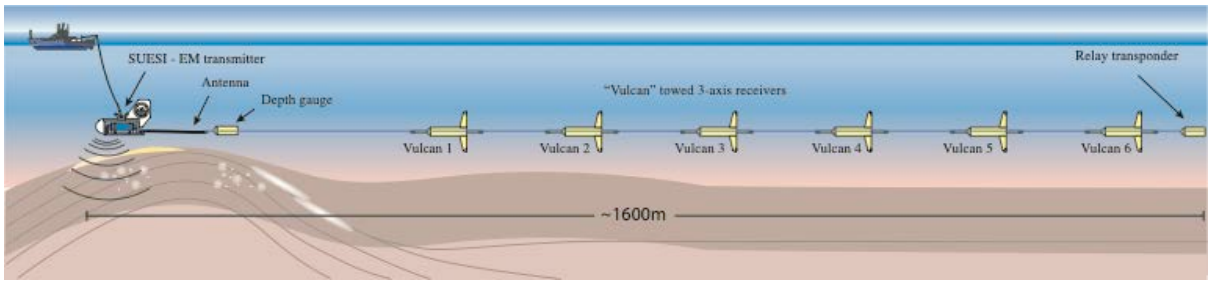

Figure 7.1 Example of SUESI deployed with Vulcan receivers.

SUESI is attached to the 0.680 inch coaxial deep-tow cable, through which power is sent from shipboard power supplies to SUESI. This cable is also used to communicate with SUESI, and SUESI reports operational parameters and array telemetry back to operators on board the ship. Trailing behind SUESI is a 100 m dipole antenna with 10 m copper electrodes. Also being towed behind SUESI is the Vulcan receiver array. This array consists of nine instrument packages, including six Vulcan receivers and one altimeter, and two acoustic transponder systems. Real-time telemetry is sent back to operators on board the ship who monitor SUESI health and altitude, array altitude and geometry, and tail-end altitude. The six Vulcan receivers are located at 600 m, 800 m, 1000 m, 1200 m, 1400 m and 1600 m behind SUESI. The SUESI transmit current was 290±5 A.

SUESI is a horizontal electric dipole CSEM transmitter designed and built by the Electromagnetics Laboratory at Scripps Institution of Oceanography (Figure 7.2). SUESI receives high voltage down a tow cable from a ship and transforms it to a high-current GPS-stabilised CSEM signal transmitted from copper electrodes at the ends of two neutrally buoyant antennas. The SUESI transmitter electronics are housed in an anodised aluminium

pressure housing rated to 6000 metres of seawater. This pressure housing is mounted in a stainless steel tow frame with a stabilising fin and several peripheral devices. These include a conductivity, temperature and depth (CTD) unit, acoustic altimeter and a telemetry system for communicating with receivers and navigation devices towed behind the SUESI. Either long baseline or short baseline acoustic systems are mounted to the SUESI frame for navigation.

Figure 7.2 SUESI transmitter on deck, without antennas attached.

The SUESI tow frame is towed behind a 0.680 inch (17 mm) coaxial tow cable. The tow cable has a working load limit of 10,000 pounds and is used to send up to 2000V RMS to SUESI, as well as two-way telemetry at 9600 baud. During deep tow operations, the SUESI tow frame is 'flown' at a constant altitude above the seafloor by paying out and hauling in on the coaxial tow cable with a hydraulic winch. On the ship side, the tow cable terminates in a high-voltage slip ring mounted to the winch. On the other end of the cable, a custom mechanical and electrical termination connect to the SUESI.

The high-voltage power delivered to SUESI via the tow cable is supplied by a 30 kVA Elgar/Ametek power conditioning unit (Figure 7.3). The Elgar/Ametek takes 208-500 VAC three-phase power from the ship and outputs up to 2000V, which is GPS-stabilised at 400 Hz.

Figure 7.3 Elgar power supply.

Prior to deploying the SUESI CSEM array, all Vulcans and tail-end transponder systems were synced, started, sealed and vacuumed. Copper electrodes for the long SUESI antenna were cut to length and ready to install. The copper electrode on the short SUESI antenna was pre-installed and configured with a drogue. The SUESI waveform phase is GPS-locked and was synced to GPS time every time SUESI was powered up (see Table 7.1 for sync times).

Table 7.1 Times of synchronisation to GPS.

Year	Month	Day	Ordinal Day	Hour	Minute	Second	Tag
2020	11	1	306	20	1	0	0.001636
2020	11	2	307	2	40	0	0.001674
2020	11	4	309	1	58	0	0.001659
2020	11	5	310	6	54	0	0.0016
2020	11	7	312	1	44	0	0.001617
2020	11	10	315	14	53	0	0.001642
2020	11	10	315	22	58	0	0.001649

Navigation of the array can be performed using either an inverted long baseline system, called Barracudas, or the ultra-short baseline (USBL) HiPAP transponder system (Section 7.6) with cNode beacons attached to SUESI. In practice, the USBL system was easier to use and created less acoustic noise than the Barracuda system.

Upon recovery, CSEM data were downloaded from each logger and spectrograms constructed for each channel of each logger. Figure 7.4 shows an example of a spectrogram from a single Vulcan, 'Mahi', from the first deployment. The first channel is the horizontal crossline dipole, perpendicular to the tow direction, which, with the given transmitter orientation, will have little to no signal present. The inline dipole channel is the second channel and shows considerable signal on the transmitted 0.5 Hz fundamental and associated harmonic frequencies. The third channel is the vertical dipole, and, while weaker than the inline channel, the signal is readily apparent. Even though the signal is weaker, this channel is particularly sensitive to vertical features, like seeps. The final and fourth channel shows the timing signal, which is a sample of the transmitted waveform taken at the transmitter that is then sent down the telemetry cable to the logger. With this, we can achieve very accurate timing, which is necessary for accurate interpretation of processed phase data. These spectrograms show the quality of the data and that data was successfully recorded – something that is unknown until recovery of the loggers. However, no geologic interpretation can be inferred from these spectrograms. Interpretation requires Fourier decomposition of the time series for each channel, at which point modelling, either forward modelling or inversions, are performed on the ensemble dataset.

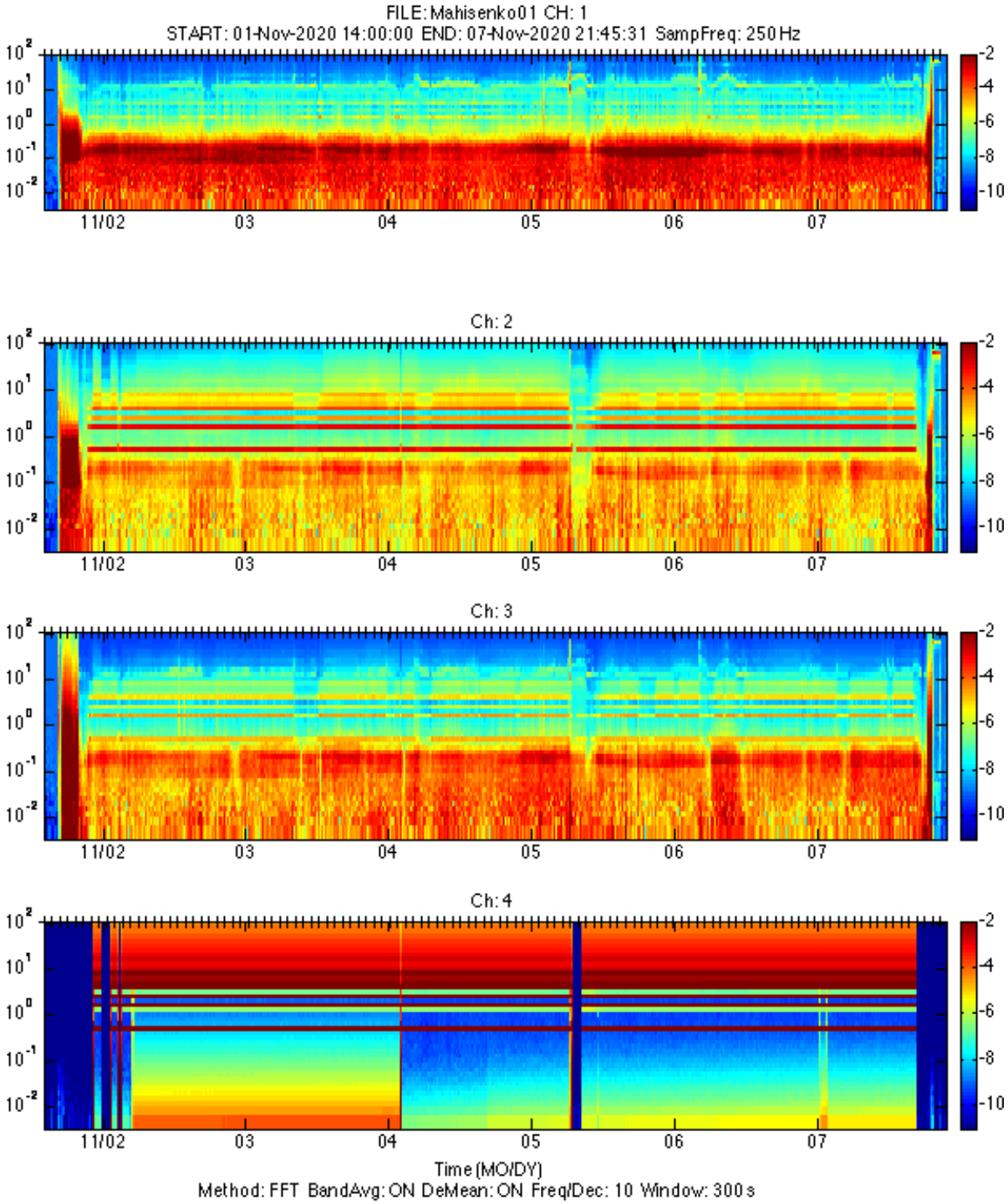

Figure 7.4 Spectrogram of four channels from a single logger. Channel 1: crossline dipole, Channel 2: inline dipole, Channel 3: vertical dipole, Channel 4: timing signal.

The transmitted signal can be easily seen in the time series of each channel, as shown in Figure 7.5. While a square wave is transmitted, by the time the signal reaches the receiver, the high-frequency content of the waveform is attenuated, causing the recorded waveform to appear rounded, with a sharkfin-like appearance. The power spectrum (Figure 7.6) shows the relative difference between the noise floor and signal at the fundamental frequency (0.5 Hz) and the resulting harmonics. In a standard square wave, harmonic amplitude falls off geometrically. By modifying the square wave, we are able to push increased energy into the higher frequencies, providing better depth resolution when the data are inverted.

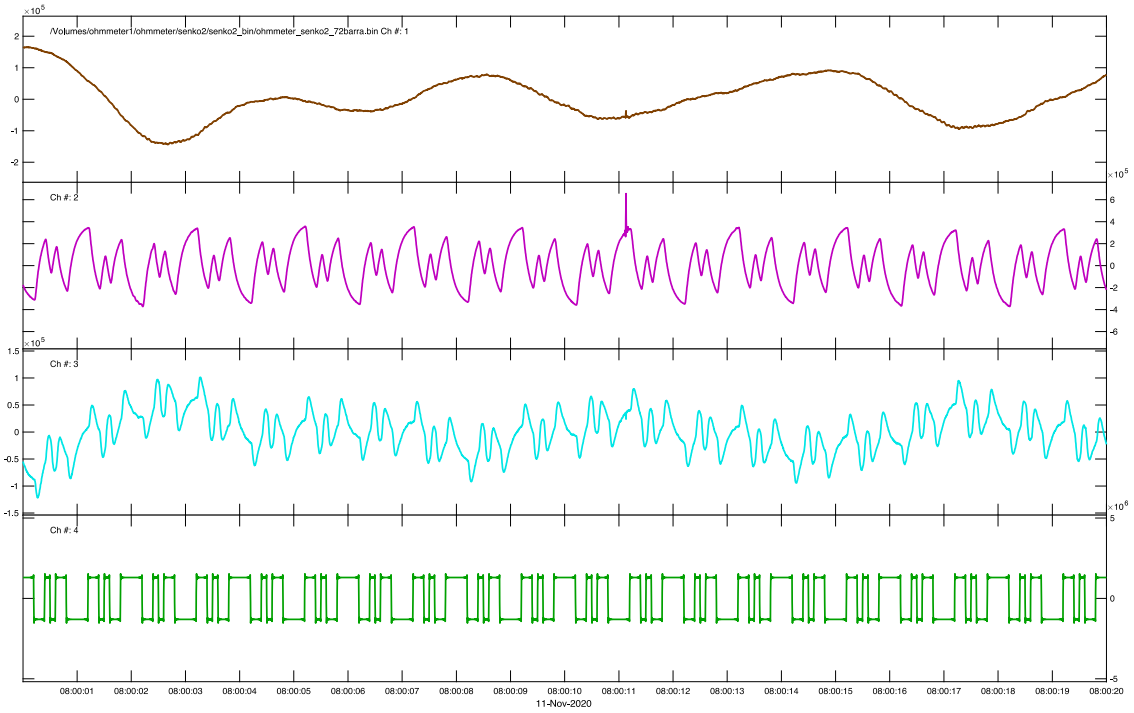

Figure 7.5 Time series showing the three electric field dipoles (top three plots), as well as the timing pulse on the bottom plot.

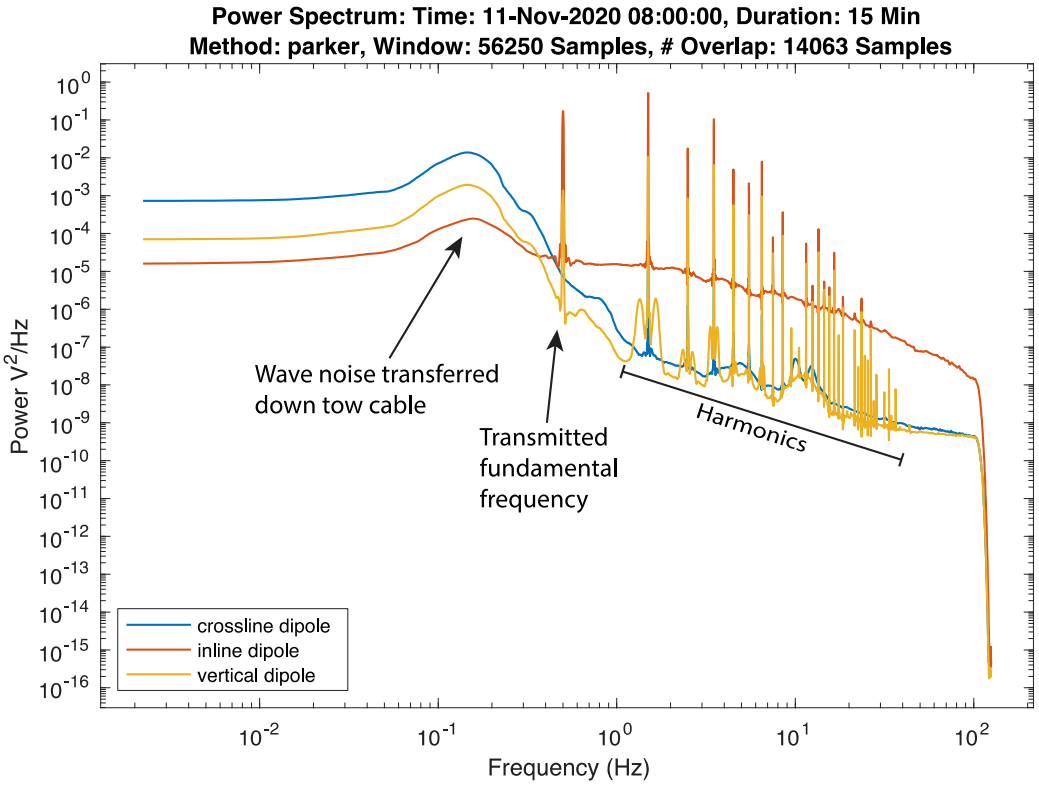

Figure 7.6 Power spectrum for the three electric field channels. Across many frequencies, the power of the inline and vertical channels are many orders of magnitude above the noise floor.

7.2 Kongsberg Simrad EM302 Multibeam Echo Sounder

7.2.1 Set-Up

A hull-mounted Kongsberg Maritime EM302 MBES was used to obtain swath bathymetry, backscatter and water column data during TAN2012.

The EM302 MBES is a high-resolution seabed mapping system for water depths of 10 m down to 7000 m. This echo sounder operates at a frequency of 30 kHz, with an angular sector of 140°, across track coverage of 3–5 times water depth (depending on depth and mode) and a maximum ping rate of 10 Hz. The system dynamically applies beam focusing to both transmit and receive functions in order to obtain the maximum resolution inside the acoustic nearfield. The transmit beams are electronically stabilised for roll, pitch and yaw, while the receive beams are stabilised for roll movements. As configured on *RV Tangaroa*, the EM302 is a 1° TX by 2° RX system with 288 beams (or 576 beams in dual swath mode) yielding 432 soundings (or 864 soundings in dual swath mode), with beam spacing being equidistant or equiangular. In order to increase the maximum useful swath width, the EM302 uses both continuous wave (CW) pulses and frequency-modulated (FM) sweep pulses with pulse compression on reception. The transmit fan is split in several individual sectors with independent active steering to accomplish compensation for the vessel motion (pitch, roll yaw and heave), supplied in real time by the Applanix POSMV.

In dual swath mode (two swaths per ping), the transmit fan is duplicated and transmitted with a small difference in along-track tilt. The applied tilt considers depth, coverage and vessel speed to give a constant sounding separation along track. System operating parameters are given in Table 7.2.

The EM302 is equipped with a soft start function allowing for a slow ramp-up in power on start-up and the ability to operate with reduced transmission power, in order to mitigate any potential harmful effects on marine mammals.

Table 7.2 Summary of EM302 operating parameters for TAN2012.

Type of Instrument	**EM302**
Frequency	30 kHz
Maximum ping rate	Auto / set by K-Sync when in combination with TOPAS sub-bottom profiler and ES60 single-beam
Beam spacing	HD Equidistant Beam Spacing
Angular coverage mode	Auto
Number of beams per swath	288
Number of swaths per ping	2, giving a total of 576 beams per ping
Number of soundings per ping	864
Nominal depth range from transducers	10–7000 m, with typical values for this survey of 100–2800 m
Beam width	1.0° x 2.0°

Type of Instrument	EM302
Coverage	8000 m nominal max (4000 m each side, fixed for this survey), ranging from 80 to 7600 m for this survey with a typical value of approximately 2800 m (1400 m / side)
Coverage sector	50–65° per side maximum (for this survey)
Depth resolution	0.25% of water depth
Ping mode	Auto: shallow, medium and deep, depending on depth for this survey
Beam forming method	CW (FM disabled)
Range sampling rate	45 kHz
Pulse length	Auto: 5 ms
Dual swath	Dynamic
Pitch stabilisation	Enabled
Auto-tilt	Off

Seafloor Information System (SIS) version 4.3.2 was the real-time software application used onboard the vessel for multibeam data acquisition. This software includes the necessary features for running and operating the multibeam system. It includes extensive tools for visualising the sounding data, as well as the seabed image data, and enables checks on system calibration and data quality to be made in real time. Figure 7.7 provides an example of the controls and options available within the SIS interface.

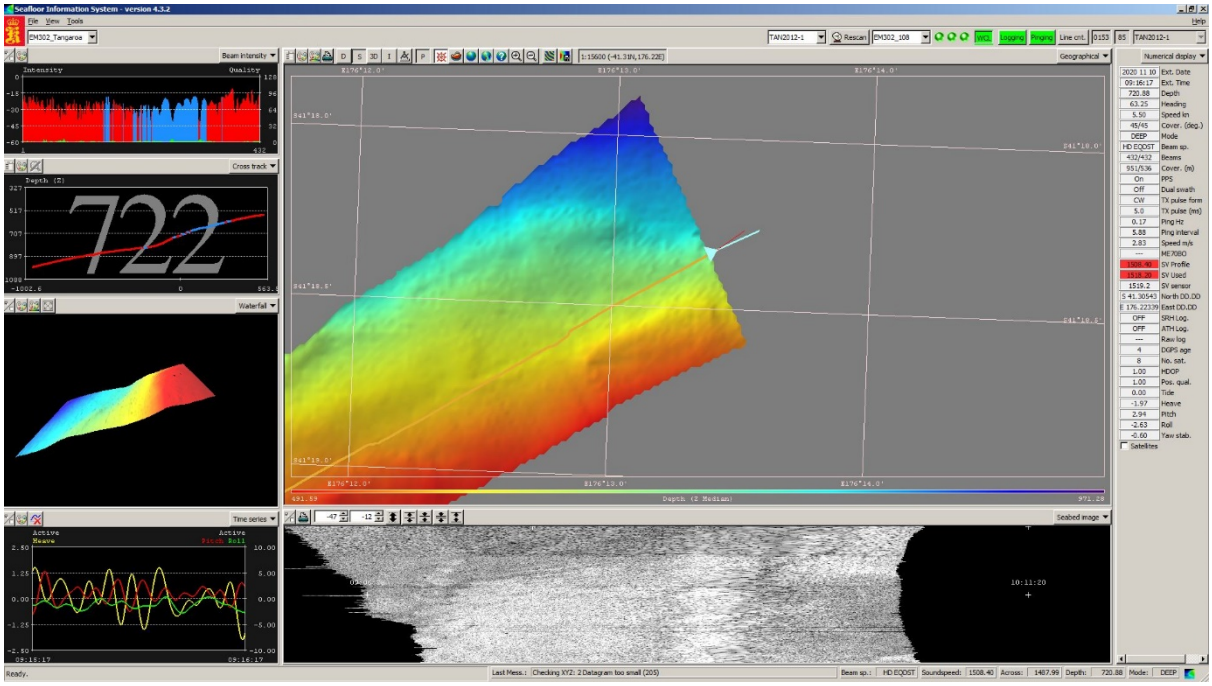

Figure 7.7 Example of the Seafloor Information System interface used for control of MBES acquisition during TAN2012. Starting from top left in counter-clockwise order: sub-windows show beam quality; waterfall of seafloor solution; heave, pitch and roll fed in from POSMV; seafloor reflectivity (backscatter); control parameters of survey; and real-time seafloor solution from collected bathymetry data.

In addition to the slant-range information incorporated in the bathymetric data, the EM302 also records, for each beam, the amplitude of the returned acoustic signal relative to the amplitude of the emitted pulse. This amplitude data forms the basis for the generation of backscatter snippets and the visualisation, classification and analysis of the compositional provinces likely present on the seafloor. This backscatter data was recorded simultaneously with the bathymetric data and was viewable in real time through the SIS interface, as illustrated in Figure 7.8, enabling active control of data integrity.

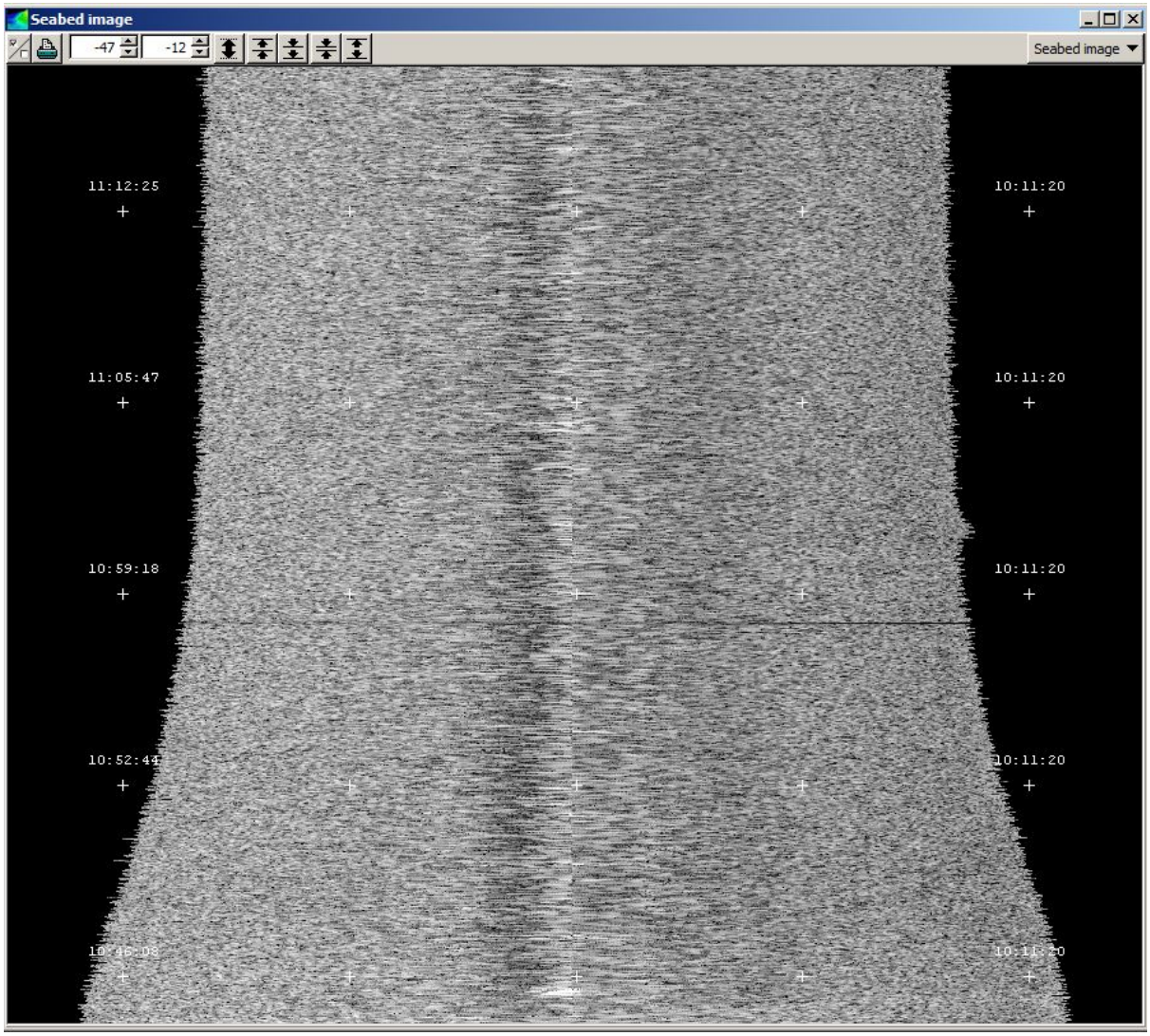

Figure 7.8 Example of the real-time visualisation of the acoustic amplitude of seafloor returns (i.e. backscatter data) in the Seafloor Information System interface in the Seabed Image window during TAN2012.

The EM302 MBES is also capable of detecting the acoustic return from midwater reflectors, and, for TAN2012, this water column data was logged and the received amplitudes of the entire water column for each beam recorded simultaneously with the MBES bathymetric data. Like the backscatter data, the collection and quality of water column data was viewable in real time through the SIS interface (Figure 7.9).

As reference water column sound velocity profiles could not be acquired for TAN2012, profiles from *World Ocean Atlas 2013 version 2* (WOA13 V2) were used. These profiles were used to calibrate and correct travel times, ray paths and water depth in the MBES data (Table 7.3). The results provided a good match to results from the TAN1808 voyage (Crutchley et al. 2018b) in the same area.

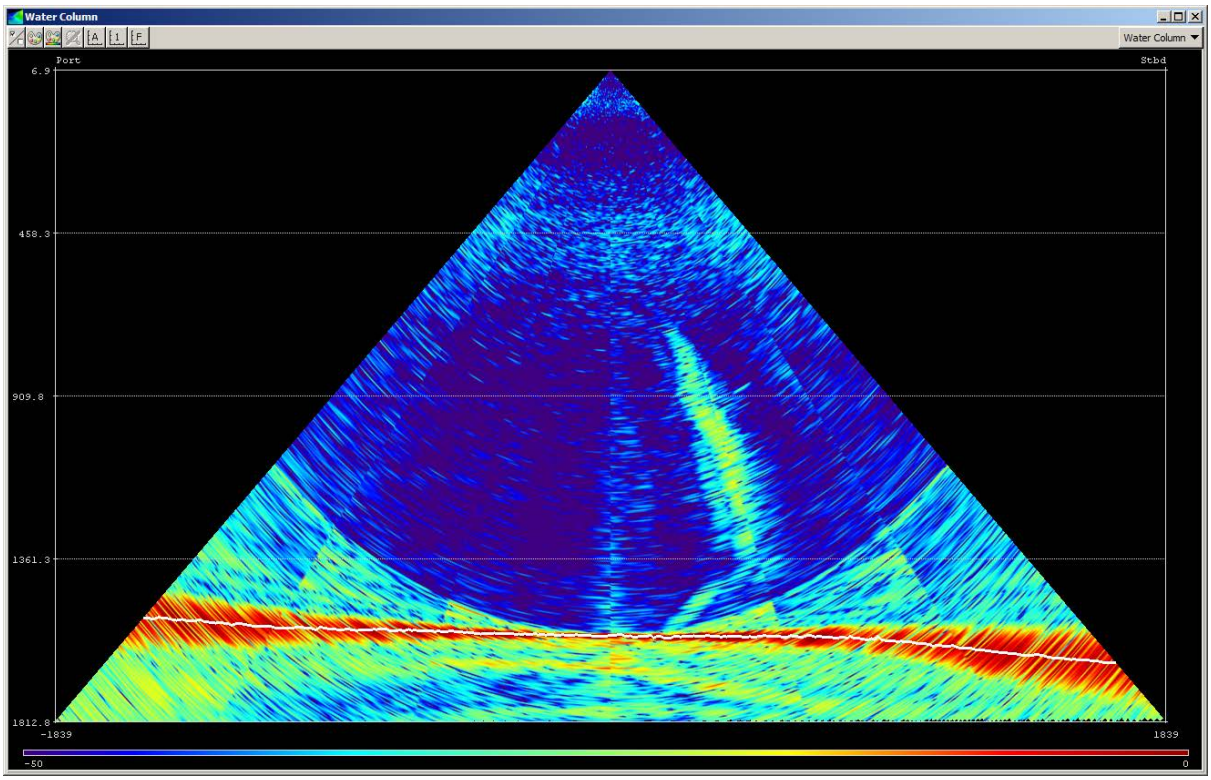

Figure 7.9 Example of the real-time visualisation of the water column data during TAN2012 in Kongsberg Maritime's Seafloor Information System showing a prominent flare. The Y-axis represents depth and the X-axis represents coverage, both in metres, while the white line represents the detected depth curve (i.e. the seafloor).

Table 7.3 Date, time, position and depth of eight sound velocity profiles generated from the World Ocean Atlas 2013 V2 during TAN2012.

File Name	Date	Time (UTC)	Latitude(S) Decimal Degrees	Longitude (E) Decimal Degrees	Profile Depth (m)
WOA13_20201102_050000	02-11-2020	05:00	-41.973	175.177	2700
WOA13_20201102_080000	02-11-2020	08:00	-41.8687	175.4997	2700
WOA13_20201102_120000	02-11-2020	12:00	-41.8145	175.6698	2700
WOA13_20201102_213500	02-11-2020	21:35	-41.41	175.56	2700
WOA13_20201103_080000	03-11-2020	08:00	-41.61	175.1536	2699
WOA13_20201107_230000	07-11-2020	23:00	-41.4819	175.2228	2800
WOA13_20201109_050000	09-11-2020	05:00	-41.5166	175.1	2800
WOA13_20201111_111111	11-11-2020	11:11	-41.6163333	176.5966166	2800

The data quality of the collected multibeam data, including backscatter and water column data, is moderate. Noise generated from the unsynchronised USBL system was present throughout the whole voyage. The USBL system was used to navigate the CSEM array, instead of the Scripps Institution of Oceanography Barracuda paravane system, which was turned off and recovered on the first day of CSEM data acquisition. The USBL system also produces noise but has fewer active sources in the water, so is overall an acoustically quieter system to use.

7.2.2 Bathymetry Processing

Raw bathymetric data were acquired using a Kongsberg Maritime EM302 MBES in conjunction with Kongsberg's SIS version 4.3.2, as noted above. Files of soundings (**.all* format) from each completed transect were imported into QPS Qimera 2.2.5 software for initial processing (Figure 7.4). A standard Qimera workflow was followed prior to the rendering of bathymetric data as a surface and a georeferenced raster in **.tiff* format. A tide correction was not applied. An example of the Qimera Software interface is shown in Figure 7.10.

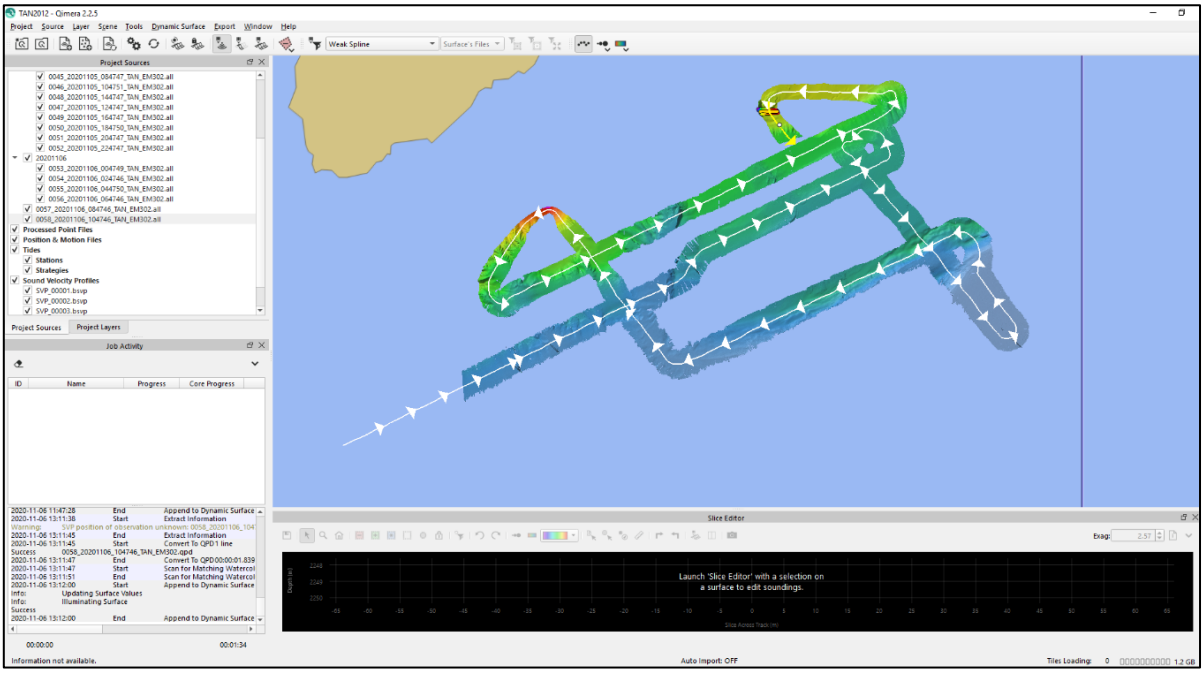

Figure 7.10 Qimera software interface with multibeam tracks and data handling sub-windows as used during TAN2012 for the examination of bathymetry.

Before exporting the surface into a georeferenced format, the data were edited on a line-by-line basis using the Swath Editor tool. Bathymetric soundings that represented gross errors or obvious noise were manually rejected. An example of the Swath Editor for flagging erroneous soundings to be rejected is provided in Figure 7.11. Following editing, each amended sonar file was saved and automatically updated in the dynamic surface. The final exported raster (**.geotiff*) has a cell size of 50 m.

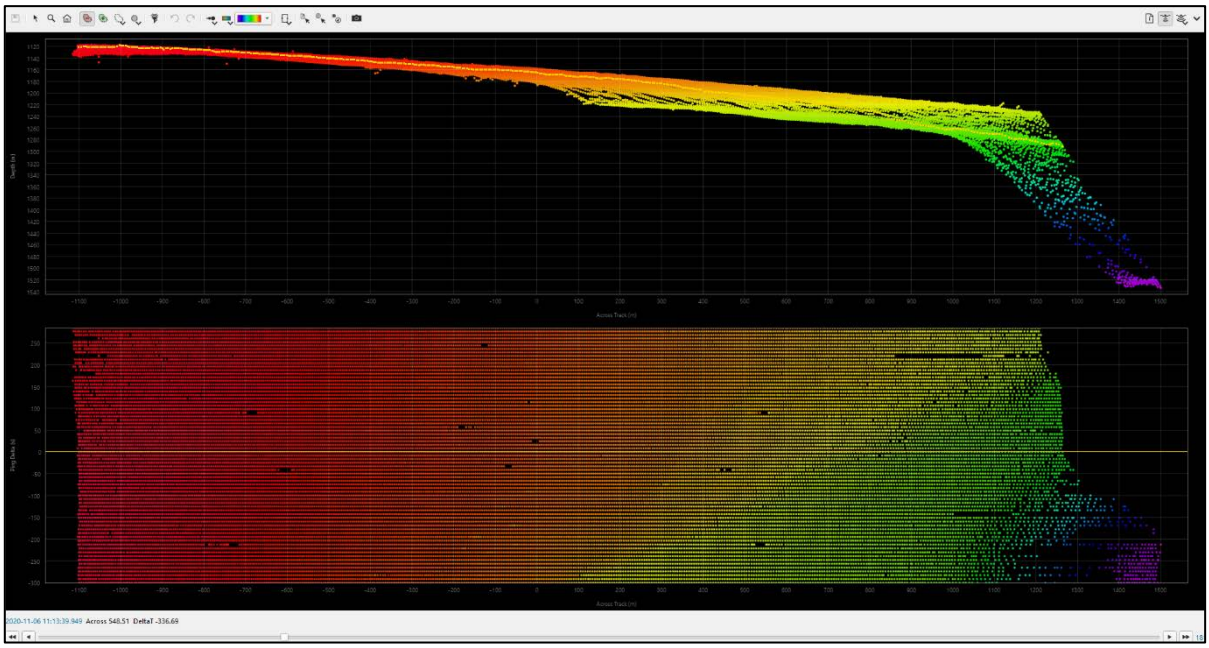

Figure 7.11 Qimera Swath Editor interface for editing bathymetry and rejecting erroneous soundings. Top: Side view of MBES data. Bottom: Rear view of MBES data.

7.2.3 Backscatter Processing

As noted in Section 7.2.1, in addition to the slant-range information incorporated in the bathymetric data, the EM302 also records, for each beam, the amplitude of the returned acoustic signal. This amplitude is recorded in the **.all* files and provides the basis for backscatter analysis. For TAN2012, the **.all* files were imported into the Fledermaus Geocoder Toolbox software program (FMGT) and rendered for initial quality control (Figure 7.12). No further processing was undertaken.

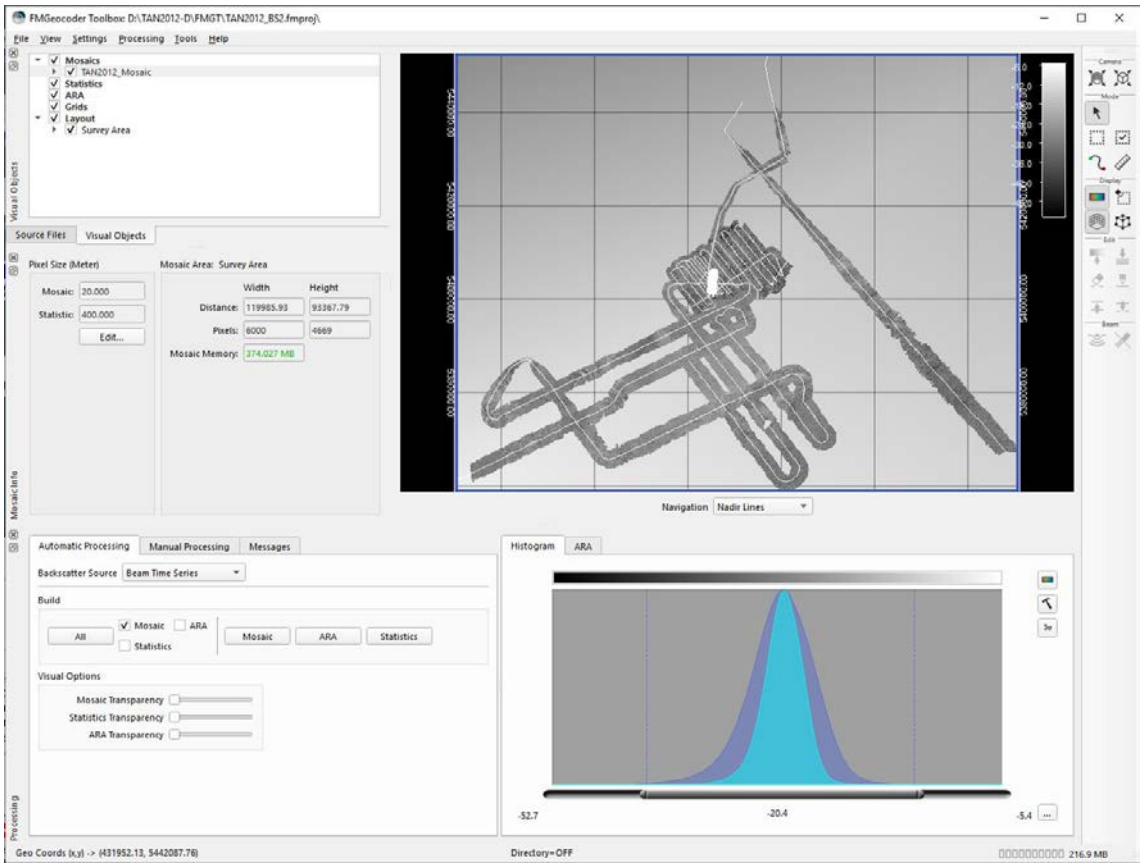

Figure 7.12 Fledermaus Geocoder Toolbox interface, which enabled the visualisation of the MBES amplitude data and backscatter, as well as the adjustment and alteration of mosaic and processing parameters during TAN2012.

7.2.4 Water Column Data Processing

In addition to slant-range and seafloor return amplitude data, the EM302 was also capable of detecting and recording the acoustic returns of mid-water reflectors. The water column data logged by the EM302 MBES (as **.wcd* files) during TAN2012 were imported into the Fledermaus Mid-Water program (FMMW) where, when combined with similarly imported **.all* files (providing navigation), they were converted to a FMMW proprietary file format (**gwc*), visualised and further processed. From the FMMW user interface (Figure 7.13), the water column data could be viewed as along-track curtains (swath) or by entire line. Typically, the entire line was viewed from the side as range-stacked (R-Stack) or depth-stacked (D-Stack) soundings, with the ability to zoom in on desired sections of the record, although the swath view was frequently employed to verify the nature of water column features. Throughout TAN2012, water column features, particularly flares, were identified. The water column data collected during TAN2012 were of generally good quality, though they suffered, like the other data collected with the EM302, from noise generated by the positioning system used with the CSEM. Noise also occurred when wind exceeded 25 knots, when swell was greater than 3–4 m and when bubble-sheeting obscured the transducer face.

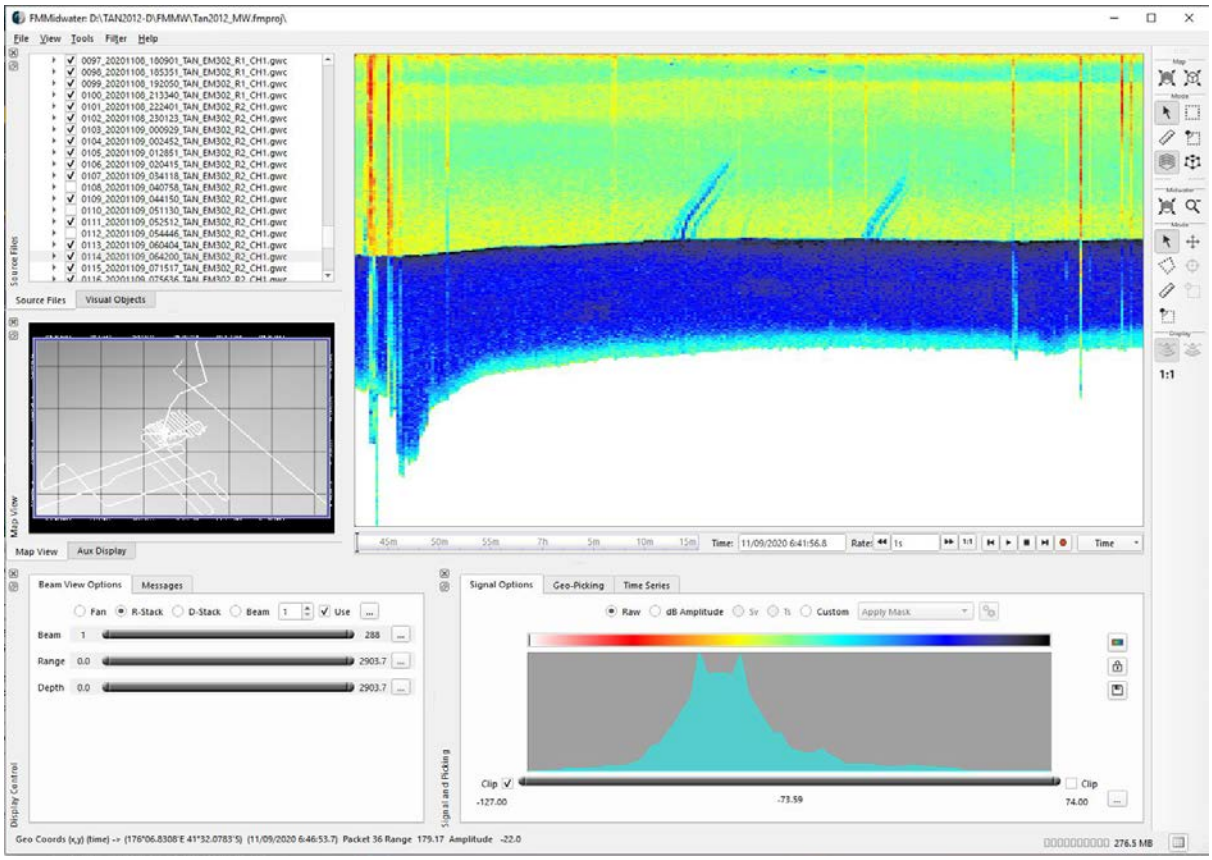

Figure 7.13 The user interface of Fledermaus Mid-Water, displaying the selected line (in which two flares are visible), its geospatial location, amplitude spectrum, beams visible, range and depth.

7.3 Motion Sensor

Throughout TAN2012, an Applanix POSMV V5 (a global navigation satellite system [GNSS]-aided inertial positioning and orientation system comprising a processing unit, an inertia measurement unit and two GNSS antennas) was used to constrain heave, pitch, roll and heading. The system has a heave accuracy of +/- 5 cm, or 5% of the range, a pitch and roll accuracy of 0.02° and a heading accuracy of 0.02°.

7.4 K-Sync Unit

The Kongsberg K-Sync unit provided synchronisation and timing between the various echo sounders used on TAN2012 to avoid interference between sounders of similar frequencies, principally the EM302, the TOPAS and the EK60 sounders, although, typically, echo sounders that do not affect each other can be placed in groups. An example of typical shot-synchronisation periods in 1900 m of water during TAN2012 is as follows: EM302 MBES (6.231 s) followed by TOPAS SBP (2.759 s) followed by EK60 (2.8 s) – repeating.

7.5 Kongsberg TOPAS PS 18 Sub-Bottom Profiler

The TOPAS Sub-Bottom Profiler (SBP), permanently mounted on the ship's starboard hull and controlled with software by the multibeam operators, was used to acoustically image the strata and structure in the seafloor's shallow sub-surface (with maximum crustal penetration of approximately 120–150 m). The transmitted waveform used during TAN2012 was a linear frequency-modulated chirp (LFM) that was externally triggered with K-Sync to avoid interference with the EM302 and other echo sounders. The frequency range of the chirp used

throughout the survey was from 2.0 to 6.0 kHz, with a chirp length of 20 ms. Transmitter output level was set to 0 dB, providing a manufacturer's maximum output level of 100%; the receiver gain was set to 0 dB and the receiver high-pass filter was set to 1.0 kHz. The TOPAS PS 18 beam is stabilised for heave, roll and pitch movements via motion data fed from the POSMV. In addition, a 'Master Depth' is provided from the EM302 MBES to aid the 'bottom track' function. The acoustic beam can also be steered manually or automatically – when slope is available from the MBES system – to consider bottom slope. However, only the manual beam steering option was used, with both pitch and roll set to 0.00 degrees during TAN2012 to ensure trace imaging and positioning continuity. Data quality was severely compromised when dynamic positioning was active (mainly during the first day of CSEM deployment). TOPAS operating parameters are given in Table 7.4, while Figure 7.14 illustrates the user interface of Kongsberg's TOPAS sub-bottom profiler.

The returned trace data were recorded in RAW format with no additional processing, other than receiver gain and the initial high-pass filter. The RAW data was converted into unprocessed *sgy* files with no processing other than the matched filter and a constant gain.

Table 7.4 TAN2012 TOPAS operating parameters.

Control	Setting	Comment
Data Collection		
Trigger mode	External (K-Sync)	Timed with EM302 and EK60 echo sounders
Pulse form	Chirp (Linear Frequency Modulation)	-
Chirp frequency	2.0–6.0 kHz	-
Chirp length	20 ms	Optimised for bottom type and water depth
Transmitter output level (power)	0 dB (maximum)	-
Heave/Roll/Pitch (HRP) stabilisation	Auto	From primary POSMV
Delay control	Automatic	Set to manual only if bottom-lock is lost
Upper/Lower delay	10% / 40%	-
Delay offset	0 ms	-
Sample rate	40 kHz	-
Trace length	250 ms	-
Gain	0 dB	Optimised for bottom type and water depth
High-pass filter	1.0 kHz	-
Sound speed	Referenced to EM302 velocity sensor (typically 1495–1505 m/s)	Stand-alone underway AML SV Plus sound velocity profiler in bow-thruster room
Initial Processing		
Bottom tracker	Enabled	-
Filters	Matched, corner frequencies high-resolution	-
Gain (digital)	3–12 dB, for almost all cruise constant at 12	Optimised for bottom type and water depth
Data-logging	Raw matched signal to SEGY	Raw **.sgy* output

Control	Setting	Comment
Display Only		
Time-varying filter	Disabled	Optimised for bottom type and water depth
Time-varying gain	Variable, bottom-tracked	-
Attribute processing	Instantaneous amplitude	For monitor display only

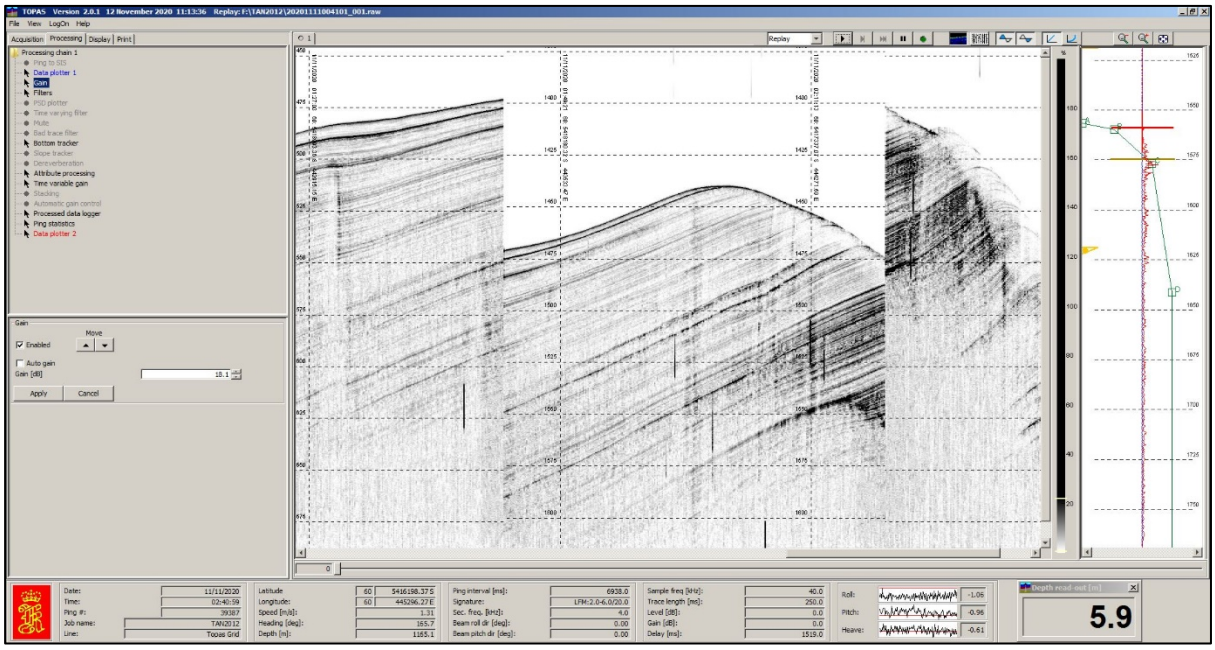

Figure 7.14 User interface of the Kongsberg Maritime TOPAS PS 18 employed during TAN2012. Sub-windows from left to right showing recording/processing parameter control, processed sub-bottom echogram and single trace display.

TOPAS processing pre-recording was kept at a minimum, similar to voyage TAN2006, consisting of a match filter and constant gain.

On-board processing was conducted using Seismic Unix and consisted of coordinate conversions, some header manipulation, instantaneous amplitude extraction and a time-variant gain. Table 7.5 lists the datasets that were generated onboard.

Table 7.5 Datasets generated onboard. Please refer to information in SBP_INFO for further details.

Directory	Description
SBP_INFO	Information, scripts, navigation, miscellaneous files.
SBP_SEGY	SEG-Y files generated by acquisition software, NZTM.
SBP_SEGY_UTM60S	NZTM in headers converted to UTM60S. [1]
SBP_SEGY_PROC	SBP_SEGY, processed. [2]
SBP_SEGY_UTM60S_PROC	SBP_SEGY_UTM60S, processed.
SBP_SEGY_LINES • CSEM • TGRCOARSE • TGRFINE • TGRET • CSEMMER	Files merged to lines in various patterns, all UTM60S: • Long profiles usually following CSEM lines. Individual files, corrected for delay time, can be read into OpendTect. [3] • As above, coarse grid over flares. • As above, fine grid over flares. • Extension from TGRFINE to beginning of CSEM Line 9. • Long profiles usually following CSEM lines, merged, with no delay time correction. Kingdom Suite should be able to read those.
SBP*replay	Separate directory structure to check into 'replayed' files associated with problems at SOL CSEM Line 9 (see text).

[1] Key commands:

proj +proj=tmerc -I +lon_0=173E +lat_0=0N \

+x_0=1600000 +y_0=10000000 +k=0.9996 \

-f %.8f +ellps=WGS84 | \

proj +proj=utm +zone=60 +south +ellps=WGS84 \

Checked with LINZ's coordinate conversion tool: http://apps.linz.govt.nz/coordinate-conversion/index.aspx, off by up to ~0.8 m.

[2] Key steps: Instantaneous amplitude, time-variant gain t^1

Key commands: suattributes mode=amp | sugain tpow=1

[3] Determination of minimum and maximum delay time, entire line is padded with zeros from minimum delay time to maximum delay time + trace length. Note, still some traces can have >65536 samples, which is not possible for SEG-Y data. OpendTect (and probably Petrel) can handle a delay time if constant throughout the line.

The processing steps carried out onboard are listed in Table 7.6.

Table 7.6 Processing sequence.

nztm2utm.run	NZTM to UTM60S conversion
sbpproc.run	Processing, do twice (on NZTM and UTM60S)
xtrsxsy.run	Extract coordinates (UTM60S and latitude/longitude only)
mergenav.run	Generate merged navigation file (UTM60S and latitude/longitude only)
chcknav.run	Check merged navigation file
xtrtbol.run	Extract time and position, start of line, sort according to time
-	Load into QGIS to check which order of lines, compare with logs, hand edit *bol_temp.csv* -> *llistX.csv*, assign line names to SBP file names (most recent, *llist6.csv*)
sbpshln.run	Assign line names, shift data according to delay time
sbpmerge.run	Read and merge SBP SEG-Y files, without any correction for delay time

Header manipulation was minimal. CDP (byte 21) was set to reel number (byte 9) to allow easier upload into interpretation software. All coordinates are in decimetres. Typical header values are shown in Table 7.7.

Table 7.7 Typical header for raw data in SBP_SEGY, *20201102160006_002.sgy* and for equivalent processed data, showing first trace. Please refer to Seismic Unix documentation for header variables.

Raw	tracl=6024 tracr=1 fldr=6024 ep=6024 cdp=1 trid=1 nvs=1 nhs=1 duse=1 sdepth=586 swdep=221734 scalel=-100 scalco=-10 sx=18264644 sy=53700665 counit=1 delrt=2907 ns=10000 dt=25 gain=1 corr=2 sfs=2000 sfe=6000 slen=20 styp=1 tatyp=3 lcf=2 lcs=6 hcs=6 year=2020 day=307 hour=16 sec=6 timbas=4
Processed (UTM 60S)	tracl=6024 tracr=1 fldr=6024 ep=6024 cdp=6024 trid=1 nvs=1 nhs=1 duse=1 sdepth=586 swdep=221734 scalel=-100 scalco=-10 sx=3940904 sy=53728716 counit=1 delrt=2907 ns=10000 dt=25 gain=1 corr=2 sfs=2000 sfe=6000 slen=20 styp=1 tatyp=3 lcf=2 lcs=6 hcs=6 year=2020 day=307 hour=16 sec=6 timbas=4

Information for interpretation software:

- Kingdom Suite should be able to read the lines in CSEMMER. cdp (Byte 21) and delrt (delay time; Byte 109) are in their standard positions. For the shorter lines, see below.
- OpendTect (tested) and probably Petrel should be able to read the files in CSEM, TGRCOARSE, TGRFINE, TGRET. Note: lines 20201105064703_016 (5a-2), 20201107024709_038 (8a-1) and 20201111104100_005 (9-10) cannot be used (number of samples >65535). The headers may contain remnants of the static correction used for adjusting for delay time changes.
- If there are unexplained errors with reading the data, check the binary headers (and compare to trace headers). This could not be done onboard.

A few notes:

- Because Seismic Unix does not use them, EBCDIC headers are meaningless; binary headers may have been compromised. However, it looks like key values in the binary headers, such as number of traces, samples and sampling rate, are correct.
- The gain was changed several times during acquisition. This has not been recorded in the headers. Gain changes should be noted in the acquisition log.

- The last line of TRGET and the first few lines of Line 9 in CSEM/CSEMMER had data gaps. This required replaying of the raw data and re-processing. It should be fixed now, but files in SBP_SEGY and SBP_SEGY_PROC have *not* been updated (files in SBP_SEGY_UTM60S and SBP_SEGY_UTM60S_PROC were updated by copying them individually). Please refer to the README_SBP_PROCESSING.txt file in SBP_INFO/scripts for details.

Figure 7.15 shows a track map of acquired TOPAS lines. Figure 7.16 is a processed TOPAS line across a cold seep site in the dense grid.

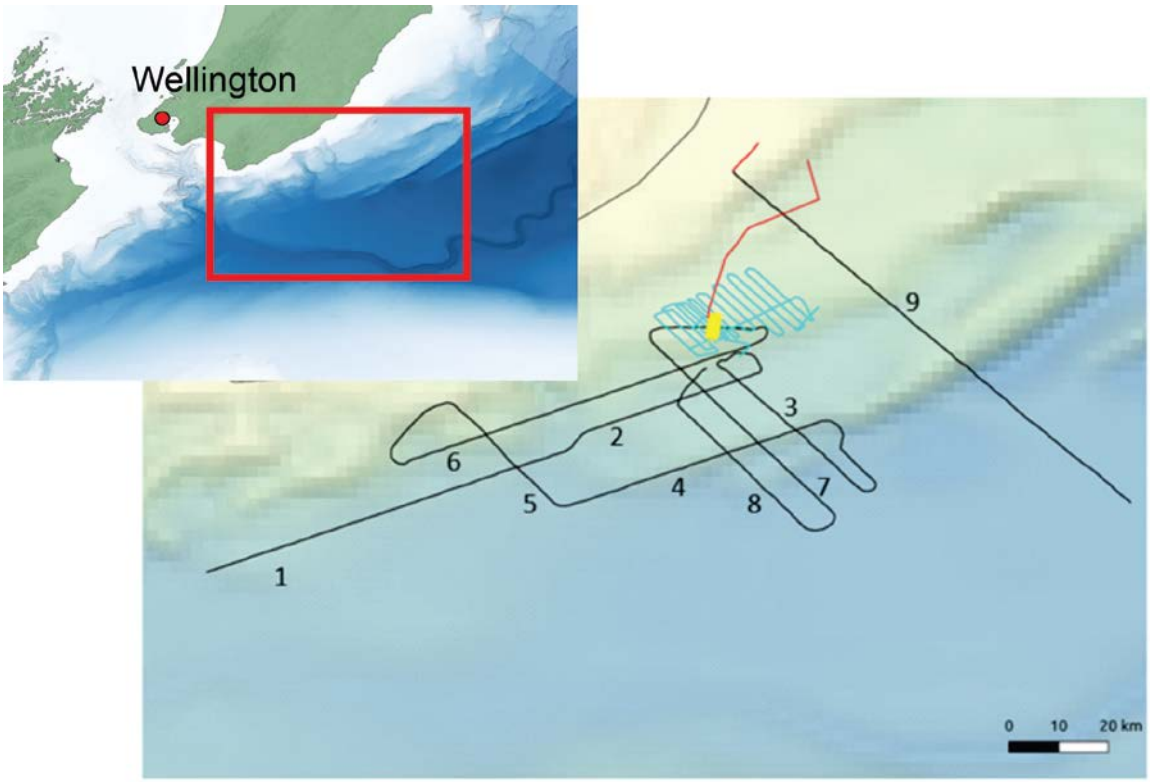

Figure 7.15 TOPAS tracks. Black: longlines largely coinciding with CSEM (CSEM and CSEMMER in Table 7.4, numbers of main lines as in TOPAS log). Blue: coarse grid (TGRCOARSE). Yellow: dense grid across cold seeps (TGRFINE). Red: extension to CSEM Line 9.

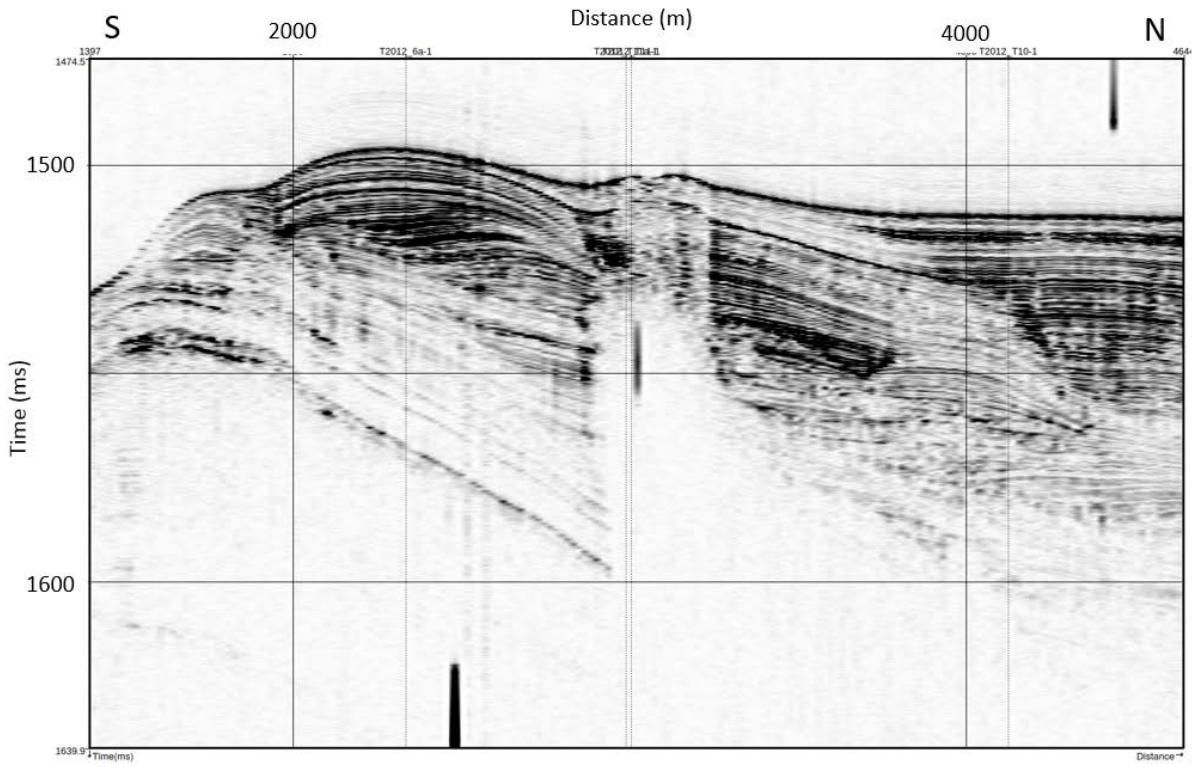

Figure 7.16 TOPAS profile from dense grid (Line 19 of TGRFINE).

7.6 High-Precision Acoustic Positioning (HiPAP) System

The *RV Tangaroa* is equipped with a HiPAP 500 system (Figure 7.17). This USBL acoustic positioning system provides the capability to calculate a geographical position for submerged objects equipment with a HiPAP transponder.

NIWA supplied three cNode MiniS 34–40V transponders with the corresponding ID codes of M03, M19 and M47 for the TAN2012. The CMS instrument was fitted with two cNode transponders, an active unit and a spare that could be activated remotely if required.

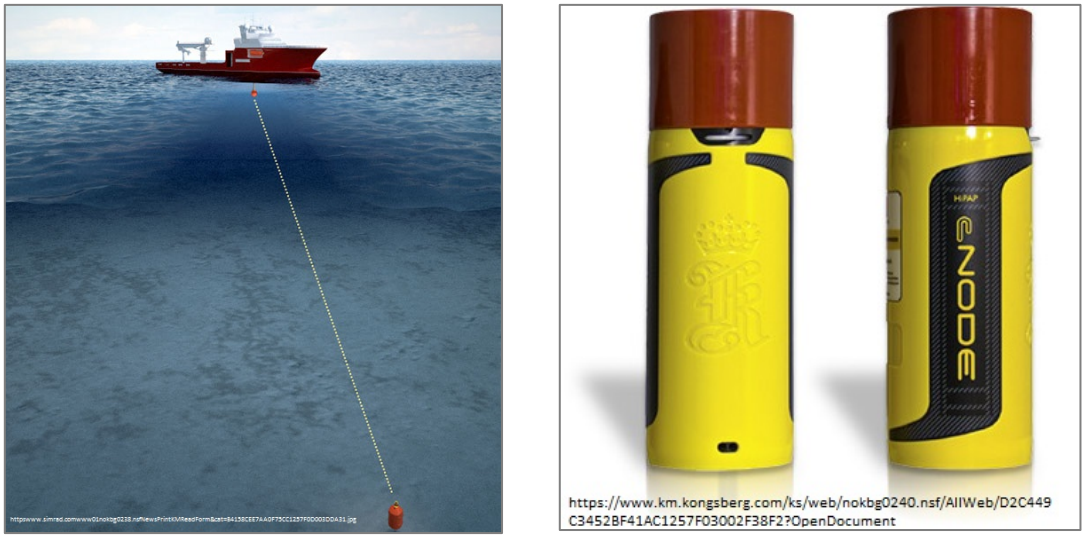

Figure 7.17 HiPAP system in operation (left); cNode transponder (right).

All HiPAP positioning was recorded during deployments. It is important to note that there is an offset in the position recorded by the NaviPac software and therefore should not be used. For correct, un-offset, positions, it is advised that either the NetCDF files or converted *.csv* files are used.

7.7 Simrad Split-Beam Echo Sounders

Simrad split-beam echo sounders were used to obtain calibrated measurements to compare with other acoustic measurements (TOPAS and Multibeam). The echo sounder data are used to detect changes of acoustic impedance in the water column, which can be caused by fish, algae, gas bubbles, etc. We collected echo sounder data to image gas flares rising from the seabed at known sites. The gas bubbles resonate at different frequencies that are mainly dependent on their size and shape. Split-beam echo sounder data are useful to be able to calculate the concentration and distribution of gas bubbles of different size and, ideally, to obtain relative or absolute methane flux rates at these sites. However, the higher the frequency of the acoustic signal, the lower the penetration of the signal in the water column – for most of the targeted flares, only the 18 kHz and 38 kHz echo sounders had enough penetration to image the gas bubbles (Figure 7.18).

The split-beam systems are regularly calibrated using a standard 38.1 mm tungsten sphere that is hung under the vessel (last calibration was done in September 2020). The EK60 18 kHz, 38 kHz, 120 kHz and 200 kHz systems are single-frequency systems, whereas the EK80 system is a broadband system that operates from 45 kHz to 90 kHz (Table 7.8).

All five Simrad echo sounders were controlled by the same transceiver computer running Simrad's EK80 acquisition application. The EK80 application was configured to wait for an external trigger from the K-sync to avoid interference with the other onboard acoustic systems. Configuration parameters such as bottom detection, displayed depth and recorded depth were adjusted each time the K-Sync trigger interval was altered to ensure that the system was able to sample data from the full water column.

Table 7.8 Frequency bands used on various platforms.

Transducer(s) Mounting	Model and Frequency Band Used
Hull (gondola)	• Simrad EK60 GPT: 18 kHz • Simrad EK60 GPT: 38 kHz • Simrad EK80 WBT: 45–90 kHz • Simrad EK60 GPT: 120 kHz • Simrad EK60 GPT: 200 kHz

The EK80 application consolidates and stores the data from all five frequencies in one raw file that can be replayed or analysed on third-party software. The raw file was stored locally and externally backed up at regular intervals to the vessel's servers.

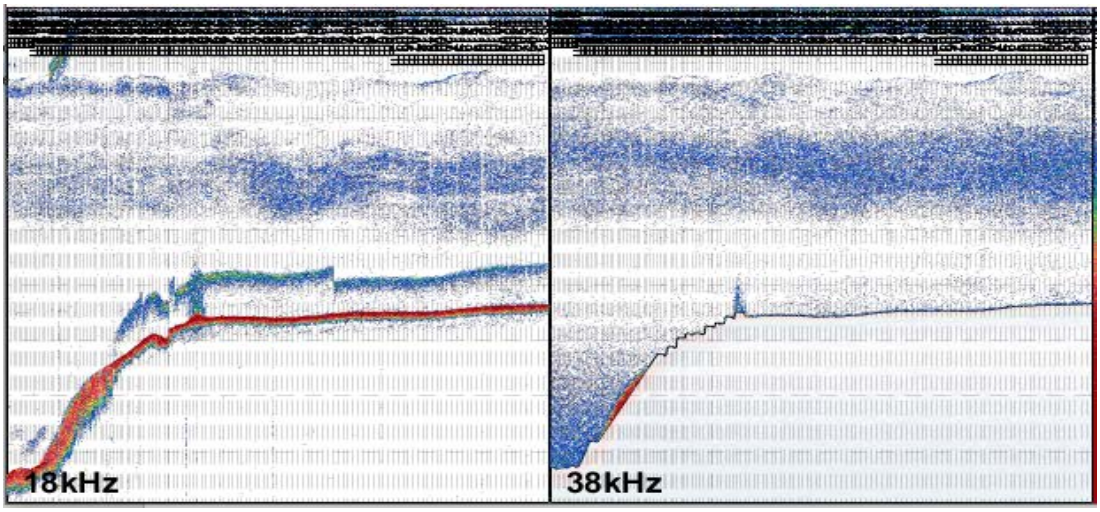

Figure 7.18 Single beam echo sounder data at 18 kHz and 38 kHz acquired in the South Hikurangi Margin in November 2020.

7.8 Data Storage

The TAN2012 voyage data are stored in the GNS Science Digital Scientific Data Media Archive (U00095). Stored data include the raw CSEM and the raw and processed TOPAS and MBES data (internal access only, contact Jenny Black, Karsten Kroeger or Jess Hillman). The TOPAS and MBES data will also be lodged with the Ministry of Business, Innovation & Employment in New Zealand.

8.0 ACKNOWLEDGMENTS

The science team is grateful to the Captain (Dan Hayward) and entire crew of *RV Tangaroa* for their excellent support during the voyage. Thanks also go to Jess Hillman, Vaughan Stagpoole, Stuart Henrys and Jenny Black for their support before and after the voyage. Funding for the ship time was provided by the Ministry of Business, Innovation & Employment (MBIE) through the Strategic Science Investment Fund. Funding of onboard operations and scientist participation was also provided by MBIE under a contestable Endeavour Research Programme (Contract C05X1708). Additionally, this work is supported by the National Science Foundation under grant number OCE-1916553. Jenny Black and Wanda Stratford (GNS Science) are thanked for reviewing this report, and Kate Robb (GNS Science) formatted this report.

9.0 REFERENCES

Barnes PM, Lamarche G, Bialas J, Henrys S, Pecher I, Netzeband GL, Greinert J, Mountjoy JJ, Pedley K, Crutchley G. 2010. Tectonic and geological framework for gas hydrates and cold seeps on the Hikurangi subduction margin, New Zealand. *Marine Geology*. 272(1):26–48. doi:10.1016/j.margeo.2009.03.012.

Crutchley GJ, Fraser DRA, Pecher IA, Gorman AR, Maslen G, Henrys SA. 2015. Gas migration into gas hydrate-bearing sediments on the southern Hikurangi margin of New Zealand. *Journal of Geophysical Research: Solid Earth*. 120(2):725–743. doi:10.1002/2014JB011503.

Crutchley GJ, Kroeger KF, Pecher IA, Gorman AR. 2018a. How tectonic folding influences gas hydrate formation: New Zealand's Hikurangi subduction margin. *Geology*. 47(1):39–42. doi:10.1130/g45151.1.

Crutchley GJ, Mountjoy JJ, Davy BW, Hillman JIT, Watson S, Stewart LC, Woelz S, Kane T, Gerring P, Quinn W, et al. 2018b. Gas hydrate systems of the southern Hikurangi Margin, Aotearoa, New Zealand. Lower Hutt (NZ): GNS Science. 83 p. (GNS Science report; 2018/40).

Fohrmann M, Pecher IA. 2012. Analysing sand-dominated channel systems for potential gas-hydrate-reservoirs using an AVO seismic inversion technique on the Southern Hikurangi Margin, New Zealand. *Marine and Petroleum Geology*. 38(1):19–34. doi:10.1016/j.marpetgeo.2012.08.001.

Fraser DRA, Gorman AR, Pecher IA, Crutchley GJ, Henrys SA. 2016. Gas hydrate accumulations related to focused fluid flow in the Pegasus Basin, southern Hikurangi Margin, New Zealand. *Marine and Petroleum Geology*. 77:399–408. doi:10.1016/j.marpetgeo.2016.06.025.

Fugro Marine Geoservices. 2015. PEP 57083, PEP 57085, PEP 57087 integrated final report: geophysical, geochemical and heat flow survey, 2015. Wellington (NZ): New Zealand Petroleum & Minerals. 24 p. Unpublished Petroleum Report PR5365.

Greinert J, Lewis KB, Bialas J, Pecher IA, Rowden A, Bowden DA, De Batist M, Linke P. 2010. Methane seepage along the Hikurangi Margin, New Zealand: overview of studies in 2006 and 2007 and new evidence from visual, bathymetric and hydroacoustic investigations. *Marine Geology*. 272(1):6–25. doi:10.1016/j.margeo.2010.01.017.

Kannberg PK, Constable S. 2020. Characterization and quantification of gas hydrates in the California Borderlands. *Geophysical Research Letters*. 47(6):e2019GL084703. doi:10.1029/2019GL084703.

Kroeger KF, Crutchley GJ, Kellett R, Barnes PM. 2019. A 3-D model of gas generation, migration, and gas hydrate formation at a young convergent margin (Hikurangi Margin, New Zealand). *Geochemistry, Geophysics, Geosystems*. 20(11):5126–5147. doi:10.1029/2019GC008275.

Kroeger KF, Plaza-Faverola A, Barnes PM, Pecher IA. 2015. Thermal evolution of the New Zealand Hikurangi subduction margin: impact on natural gas generation and methane hydrate formation – a model study. *Marine and Petroleum Geology*. 63:97–114. doi:10.1016/j.marpetgeo.2015.01.020.

Majumdar U, Cook AE, Shedd W, Frye M. 2016. The connection between natural gas hydrate and bottom-simulating reflectors. *Geophysical Research Letters*. 43(13):7044–7051. doi:10.1002/2016GL069443.

Pecher IA, Henrys SA. 2003. Potential gas reserves in gas hydrate sweet spots on the Hikurangi Margin, New Zealand. Lower Hutt (NZ): Institute of Geological & Nuclear Sciences. 32 p. (Institute of Geological & Nuclear Sciences science report; 2003/23).

Plaza-Faverola A, Pecher I, Crutchley G, Barnes PM, Bünz S, Golding T, Klaeschen D, Papenberg C, Bialas J. 2014. Submarine gas seepage in a mixed contractional and shear deformation regime: cases from the Hikurangi oblique-subduction margin. *Geochemistry, Geophysics, Geosystems*. 15(2):416–433. doi:10.1002/2013GC005082.

Watson SJ, Mountjoy JJ, Barnes PM, Crutchley GJ, Lamarche G, Higgs B, Hillman J, Orpin AR, Micallef A, Neil H, et al. 2019. Focused fluid seepage related to variations in accretionary wedge structure, Hikurangi margin, New Zealand. *Geology*. 48(1):56–61. doi:10.1130/g46666.1.

www.gns.cri.nz

Principal Location

1 Fairway Drive, Avalon
Lower Hutt 5010
PO Box 30368
Lower Hutt 5040
New Zealand
T +64-4-570 1444
F +64-4-570 4600

Other Locations

Dunedin Research Centre
764 Cumberland Street
Private Bag 1930
Dunedin 9054
New Zealand
T +64-3-477 4050
F +64-3-477 5232

Wairakei Research Centre
114 Karetoto Road
Private Bag 2000
Taupo 3352
New Zealand
T +64-7-374 8211
F +64-7-374 8199

National Isotope Centre
30 Gracefield Road
PO Box 30368
Lower Hutt 5040
New Zealand
T +64-4-570 1444
F +64-4-570 4657